# Effect of Coolant Jet Holes Direction on Film Cooling Performance

**Dr. Assim H. Yousif, Dr.Amer M. Al-Dabaghand Dr.Muwafag Sh. Alwan**

**University of Technology, Baghdad, Iraq**

**Abstract**

The film cooling effectiveness and local heat transfer coefficient for coolant jet holes direction (orientation angle), have been investigated. Experimental investigations were done on a flat plate by using a single test transient IR thermograph technique. Evaluation of the cooling performance is obtained by estimated both film cooling effectiveness and heat flux ratios. Threemodelsof coolant jet holesare investigated,each model consists of two rows of holes arranged in a staggered way with different orientation angles. Model (1) downstream row with acute angle and the upstream row with obtuse angle; model (2) both rows with obtuse angles, while model (3) both rows with acute angles.The holes diameter is 4mm, the longitudinal distance between the upstream and downstream rows (X/D) is 4D, and the span distance between two neighboring holes (S/D) is 3D.Three blowing ratios of (BR= 0.5, 1.0, and 1.5) were used in the investigation program. In order to predictthe flow behavior numerically for the cases under investigation CFDcode isintroduced.The numerical investigation shows two large vortices large counter rotating vortex pair and horseshoe vortices, both vortices have major effects on cooling performance.The experimental results showed that the film cooling effectiveness increases as blowing ratioincreases formodels (1 and 2), while decreases for model(3), and model (1) provide better performance than the others at high blowing ratios.

## تأثير أتجاه فتحات البثق البارد على الأداء الحراري لغشاء التبريد

تم دراسة تأثير أتجاه فتحات البثق البارد (زاوية الأتجاه والميل) على فعالية غشاء التبريد و معامل أنتقال الحراره الموقعي.حيث تم أجراء التجاربعملية بأستخدام تقنية الصوره الحراريه للاشعة تحت الحمراء (IR) على صفيحه مستويه بألية الفحص الأنتقالي الواحد. أن الحصول على تقييم أداء التبريد  تم بأستخدام فعالية غشاء التبريد وتقنية نسبة الفيض الحراري. وقد تم أختبار ثلاث عينات ، كل عينة من هذه العينات تحتوي على صفين من الثقوب المرتبة بشكل متعرجبزوايا أتجاه مختلفة.العينة الاولى الصف الامامي بزاوية نفث حادة والصف الخلفي بزاوية نفث منفرجة, والعينة الثانية كان صفي النفث بزاويتين منفرجتين والعينة الثالثة كان صفي النفث بزاويتين حادتين.تم تثبيت قطر الثقوب بمقدار (D=4 mm)، المسافة الطولية بين الصفين (X/D=4)، والمسافة البينية (العرضية) بين فتحات الصف الواحد بمقدار (S/D=3).أجريت التجارب بأستعمال ثلاث نسب من النفخ هي (BR=0.5, 1.0,and1.5). لتنبؤ عن سلوك الجريان تم أستخدام الحلول العددية. أعطت الأختبارات العددية المستخدمة  تنبؤ جيد لسلوك النفث البارد المحقون مع الجريان الرئيسي الحار. أن الأختبارات النظرية التي تم أستخدامها في مجال الجريان وعند منطقة التداخل بين التيارين البارد والحارأظهرت وجود

نوعين من الدوامات الكبيره، زوج من الدوامات المتعاكسة و دوامات حدوة الحصان. وقد أظهرت النتائج النظرية أن هذه الدومات تلعب دورا" رئيسيا" في التأثير على أداء التبريد. أظهرت النتائج العملية أن فعالية الغشاء تزداد بزيادة نسبة النفخ للنموذجين الاول والثاني بينما تقل للنموذج الثالث. كما أظهرت النتائج ان النموذجالاول يعطي أداء أفضل عند مقارنتهمع النموذجين الاخرين عند نسب النفخ العالية.

## Introduction

Turbine blades require better cooling technique to cope with the increase of the operating temperature with each new engine model. Film cooling is one of the most efficient cooling methods used to protect the gas turbine blades from the hot gases. Jet holes arrangement offers reliable technique help to improve the coolant effectiveness of the film cooling.

Film cooling primarily depends on the coolant-to-mainstream pressure ratio or can be related to the blowing ratio, temperature ratio ($T_c/T_m$), the film cooling hole location, configuration, and distribution on a turbine elements film cooling. In atypical gas turbine blade, the range of the blowing ratios is of about 0.5 to 2.0, while the (Tc/Tm) values vary between 0.5 and 0.85 [1].

Injecting behavior of two rows of film cooling holes with opposite lateral orientation angles have been investigated by [2] in whichhole rows arrangements were one inline and three staggered. Detailed adiabatic film cooling effectiveness distributions were measured using thermochromic Liquid Crystal to investigate how well the injecting covers the film cooled surface. They found that staggered opposite lateral arrangement shows best cooling performance.

Detailed of heat transfer coefficient and film effectiveness measurements were obtained simultaneously using a single test transient IR thermography technique for a row of cylindrical film cooling hole and shaped holes by [3]. A number of anti-vortex film cooling designs that incorporate side holes. They found that the presence of anti-vortex holes mitigates the effect the anti-vortices pairs. Experimental and numerical investigations were done by [4 and 5] to measure and topredict the film cooling performance for a row of cylindrical holes. They used adiabatic film effectiveness and heat transfer coefficents were determined on a flat plate by using a single test transient thermograph technique at four blowing ratios of 0.5, 1.0, 1.5 and 2.0.Four test designs crescent and converging slot, trench and cratered hole exits, are tested. Results showed that both the crescent and slot exits reduce the jet momentum at exit and also provide significantly higher film effectiveness with some increases in heat transfer coefficients.

Numerical prediction of [6] shows that the flow field structure of injected holes present vortices such as counter pair kidney vortex and horseshoe vortex have major effects on cooling performance, in which the strength of the kidney vortex decreases and the horseshow vortex is lifting up, leading to an improvement in the coolant performance. Therefore numerical model is suitable to design holes arrangement futures of film cooling system by introducing oriented holes row over single jet holes row.

**Experimental Facilities**

Low speed open duct test rig is used at the present investigation to supply uniform hot air to the test section as shown in figure 1. The settling chamber of the test rig contains a series of electrical heaters and row of screen to ensure adequate hot air ofuniform temperature throughout the test rig. The hot air routed through a convergent- divergent contraction having a rectangular cross-section before flowing through the test section. In order to allow the air to reach the desired temperature, the air is initially routed out away from the test section by using a by-bass gate passage. The temperature of the air is continuously monitored at the exit of the gate and when the desired temperature is reached, the gate is gradually fully opened and the hot air is passes into a test section through a rectangular duct. The operating velocity in the test section is controlled to run from 20 to 40m/s. The test section has 50mm width and 100mm height. The bottom plate of the test section is made of (234x123) mm Plexiglas of 10mm thickness and used as the test model.

A centrifugal air blower was used to supply the coolant air to the plenum. The plenum was located below the test model. The coolant air enters a plenum then ejected through holes into the test section. The coolant air pressure is measured at the inlet of the test section. Digital thermometers were used to measure the mainstream and coolant air temperature. Pre-testing showed that all holes exists constantdesired flow rate and temperature.

Two rows of staggered holes with opposite orientation angles are included in the present study. The orientation angles (Ɣ) is defined as the hole orientation toward the cross-flow in the mainstream and the inclination angle($\theta$)is defined as the angle between the centerline of the hole and the surface of the test wall as shown in figure 2. Three models at different holes direction are shown in table (1). Each model consists of two rows of holes arranged in a staggered arrangement. For model 1, theinclination angle of the upstream and downstream rows are fixed at ($\theta=30°$), and the orientation angle of (Ɣ=0°) and (Ɣ=180°) for the downstream and upstream row holesrespectively.For model 2, the jet injected angles of upstream and downstream holes are fixed at ($\theta=30°$) and (Ɣ=0°). While for model 3, the jet

injected angles of upstream and downstream holes are fixed at ($\theta$=30°) and ($\gamma$=180°). Each of holes (upstream and downstream row)contains eight holes. The holes diameter is 4mm, the longitudinal distance between the upstream and downstream rows (X/D) is 4D, and the span distance between two neighboring holes (S/D) is 3D**.** Data collected only for three middle holes for each row to reduce the effects of the side wall as shown in figure (3).

**Surface temperature measurement**

The surface temperature of test model was measured using an infrared thermographs technique. IR thermograph infrared camera type Fluke Ti32 is used at the present investigation. This camera is able to precisely record temperature variations. The IR system is greatly affected by both background temperature and local emissivity. The test surface is sprayed with mat black color to increase the emissivity like a perfect black body. The temperature measurement taken is not accurately recorded unless the IR system is calibrated.

The system was calibrated by measuring the temperature of the test surface using thermocouple type K and the reading of IR camera. The test surface is heated by mainstream hot air. The measured of temperatures obtained by both ways are recorded and stored during the heating process until achieving a steady state condition. Due to the emissivity of the test surface the temperature obtained by IR camera is differ from the temperature obtained by the thermocouple, therefore IR camera reading is adjusted until both temperatures reading are matched.

**Film cooling effectiveness and heat transfer coefficient estimation**

Consider the transient flow over a flat plate as shown in figure 4. In this casethe test plate is initially at a uniform temperature $T_i$, and the convective boundary condition is suddenly applied on the plate at time t > 0. Now, heat assumed to be conducted only in the x-direction and perform an energy balance on the plate, therefore the one-dimensional transient conduction equation is

$$\frac{\partial^2 T}{\partial x^2} = \frac{1}{\propto} \frac{\partial T}{\partial t} \tag{1}$$

The main approximation often applied to analyze transient conduction shown in Figure 4 is the semi-infinite approximation. The semi-infinite solid assumptions are valid for present investigation for two reasons. The test duration is small, usually less than 60 seconds. Secondly, the hot air flowing over the test surface made from Plexiglas of, low thermal

conductivity, low thermal diffusivity, and low lateral conduction. Therefore the solution of equation (1) as given by **[7]** is as follows:

$$\frac{T_w - T_i}{T_m - T_i} = 1 - exp\left(\frac{h^2 \alpha t}{k^2}\right) erfc(\frac{h\sqrt{\alpha t}}{k}) \qquad (2)$$

Where $T_w$ measured by using IR camera, all the other variables in the equation (2) are either known variable or measured variable except the heat transfer coefficient (h).

In film cooling case, the film should be treated as a mixture of air mainstream and the coolant air, as shown in figure 5, the mainstream temperature ($T_m$) in equation(2) has to be replaced by the film temperature ($T_f$), therefore equation (2) become as:

$$\frac{T_w - T_i}{T_f - T_i} = 1 - exp\left(\frac{h^2 \alpha t}{k^2}\right) erfc(\frac{h\sqrt{\alpha t}}{k}) \qquad (3)$$

A non-dimensional temperature term is known as the film cooling effectiveness (η), and is defined as:

$$\eta = \frac{T_f - T_m}{T_c - T_m} \qquad (4)$$

Equation (3) has two unknowns (h and $T_f$), to solve this equation, two sets of data points required to obtain the unknowns like:

$$\frac{T_{w1} - T_i}{T_f - T_i} = 1 - exp\left(\frac{h^2 \alpha t1}{k^2}\right) erfc(\frac{h\sqrt{\alpha t1}}{k}) \qquad (5)$$

$$\frac{T_{w2} - T_i}{T_f - T_i} = 1 - exp\left(\frac{h^2 \alpha t2}{k^2}\right) erfc(\frac{h\sqrt{\alpha t2}}{k}) \qquad (6)$$

In this case, a transient infrared thermograph technique will be used to obtain both h η from a single test as described by **[8]**. Thus, two images with surface temperature distributions are captured at two different times during the transient test.

A net heat flux ratio is used to measure the combined effect of film effectiveness and heat transfer coefficient **[9]**:

$$\frac{q}{q_o} = \frac{h}{h_o}\left(1 - \frac{\eta}{\phi}\right) \qquad (7)$$

The value for the overall cooling effectiveness (ø) ranges between 0.5 and 0.7.A typical value is Ø = 0.6 according to**[10]**, and this in general assumed in the present experimental analysis.

The IR images for models surface at each investigated test was captured and stored by thermal camera. These images are transferred to PC. Smart View Software program supplied with Camera can be used to limit the selected area to avoid the effect of the test section walls. The IR images converted to corresponding temperature digital values and then saved as data in Excel sheet.

MATLAB programs Software are prepared using a semi-infinite solid assumption to introduce the film cooling effectiveness and heat transfer coefficient contours. Equations, (4), (5), (6), and (7) may be solved using MATLAB Software, Smart View Software, and Excel Software. The data were collected from the selected area denoted by ($A_o$);this area included only six staggered jet holes as shown in Figure (3).

The measurement uncertainty was determined by using the methodology given by Ref. **[11]**.Error estimates for each variable are as follows: wall temperature ($\Delta T_w = \pm 2$ °C), initial temperature ($\Delta T_i$)is $\pm 2$°C, mainstream temperature($\Delta T_m$)is $\pm 0.2$°C, and coolant temperature($\Delta T_c$)is $\pm 0.2$°C. the camera frame rate is 60 Hz resulting in a time error ($\Delta t$)of $\pm 0.125\ sec$ and the test surface property($\alpha$ and $k$) uncertainty are taken from tabulated values, as a custom, $\pm 3$% relative uncertainty is assumed for both variables. The resulting average uncertainty for heat transfer coefficient and film effectiveness is ±8.2% and ±11.0%, respectively.

**Numerical procedure**

In the present study, air is taken as the working fluid and the flow characteristics are assumed to be steady flow, Newtonian fluid, incompressible fluid (Mach number=0.11), turbulent flow, three dimensional.The numerical computation area was matched to the experimental domain instead of computing only two holes with symmetry boundary conditions. FLUENT version (12.1), GAMBIT software and Auto CAD 2011will be used to create, grid for the system geometry and then simulate the film cooling for the three geometry model and three blowing ratio.The solution of the Reynolds Averaged Navier-Stokes and energy equations is obtained by usingthe commercial CFD software FLUENT is applied. Fluent is based on an unstructured solver using afinite volume approach for the solution of the RANS equations. The system geometry shown in figure 6 consists of the box with dimensions (128x12x50) mm for the hot mainstream, box with dimensions (35x12x20) mm for coolant jet and the different model geometry of two rows of holes as shown in table 1. The system geometry is drawn by using (Auto CAD 2011 code). The diameter of cooling hole is 4mm.The coolant conditions were maintained the same in all cases and the mainstream flow ratewas altered to change the blowing ratios. TheMainstream temperature was set at 322 K and the coolant temperature was set at 302 K. At the exit plane, pressure level was specified along with zero streamwise gradients for all other dependent variables.

The current study used the standard ($k - \varepsilon$) model for the simulating the turbulent flows in film cooling.The standard ($k - \varepsilon$) model is economical with reasonable accuracy for

a wide range of turbulent flows and it is widely used in heat transfer simulation**[12]**.There are some general guidelines to create a good mesh. These guidelines are shortly called rules of QRST standing for (Quality, Resolution, Smoothness, and Total cell count) **[13]**.The importance of quality parameter is the face alignment; it is the parameter that calculates skewness of cells. Elements with high skewness should be avoided.The way of checking whether the solution is grid independent or not is to create a grid with more cells to compare the solutions of the two models. Grid refinement tests for average static temperature on hot surface indicated that a grad size of approximately (2.5 million cell) provide sufficient accuracy and resolution to be adopted as the standard for film cooling system. The nodes near the test plate surface were adjusted so that average y+ value was about 20 near the test plate surface which is within the range of Ref**.[14]**.The most significant factor to be monitored for the present model is the average static temperature on hot surface. When the average static temperature on hot surface value monitor converged it is unnecessary to go further on withthe iterations and wait even if the residuals do not fall below the defined convergence criteria.

**Results and Discussion**

Figure 7 shows the contours of film cooling effectiveness for three models. The film cooling effectiveness increases with increasing the blowing ratios for model 1 and model 2, while for model 3 the effectiveness values decreases with increasing the blowing ratio. Near the hole exit and downstream, model 2 exhibit more uniformity of η values as the blowing ratios increased more than the other models for all blowing ratios. For model 3 the η contours exhibit high values of η at a hole downstream area at a low BR (BR=0.5) and η decreases with an increase in BR. This behavior only exists at model 3. Model 1 provides better performance when compared with other models at high blowing ratios (BR=1 and 1.5), because different jet holes arrangement gave different flow behavior. The behavior of flow in three dimensional domains is a complicated flow regime. To simplify the case and to make the flow recognizable and readable, the flow will be presented in two dimensions in a plane perpendicular and parallel to the cross flow at different plane location. When the coolant jet flow with the direction of hot mainstream (Ɣ=0°), multiple vortex structures are produce where two large vortex structures have been detected, counter rotating vortex pair (CVP), and horseshoe vortices. CVP plays an important role in the contribution of jet lifting off, this can be seen clearly in the case of low momentum jet (BR=0.5) and the case of high momentum jet (BR=1.5), in which the horseshoe vortex is strongly influenced by high jet momentum [6]. While when coolant jet flow opposite to the direction of hot mainstream (Ɣ=180°),the main

stream creates a local variation of pressure at the hole exit. The pressure of the injected air on the upstream side of the hole is elevated, thus locally reducing the jet velocity; and pushing up the hot stream depending on the blowing ratio.  On the downstream side of the hole, the pressure falls and locally increases the exit velocity. As the cooled air penetrate into the hot stream, its momentum decreases up to the momentum of the main stream then bend back toward the surface causing lee vortex.

The pressure variation at the hole exit create a reverse flow where part of the cooled air exits in the direction tangent and normal to rims hole  reducing the jetting effect at hole rims, which was responsible for creating kidney vortex as in the forward injection. This reverse flow creates pair of vortex similar to the kidney vortex downstream but in a plane parallel to the main stream$(CVP)_p$, this vortex is sweeping near the surface and pushing away the horseshoe vortex where moderate and wider protection area are obtained at low and high BR around the hole area.For model 1, two types of vortices are created, one $(CVP)_p$, while the second is (CVP) as shown in figure 8. For model 2 two pairs of vortices $(CVP)_p$ are appeared in a plane parallel to hot mainstream flow 1mm above the surface  as shown in figure 9. In model 3 four vortices exist in the vertical plane in the hole downstream as shown in figure 10.

As a matter of fact, the enhancement of the blade surface protection is done by keeping the local heat transfer coefficient (h) as low as possible. The local heat transfer coefficients are calculated from the data of two IR images taken in successive times.Figures 11 represents the effect of blowing ratio on local heat transfer coefficients for models (1, 2 and 3), (h) increases with increasing BR models (1 and 2), while it decreases with increasing BR for model 3. At low blowing ratios (BR=0.5), model 3 provides high heat transfer coefficient values than models 1 and 2.  As the blowing ratio increases to 1 and 1.5, model 1 gave higher heat transfer coefficient than models 2 and 3.

Figure (12a, b and c) shows $(\eta_{sa})$ variation with (X/D) for the same three models. $(\eta_{sa})$ is calculated as the average values taken from the local reading of 46 pixels in spanwise direction in twenty streamlines location downstream from the hole exist. The streamwise distance between each two successive spanwise location is (D).Model 2 shows different behavior than that of the other models as shown in figure (12 .a, b, and c), in which $(\eta_{sa})$ decreases gradually with increase in (X/D) for all BR, while in models 1 and 3, $(\eta_{sa})$ decreases and then increases.From these figures, it can be seen that any model from these models has an advantage and disadvantage. So are can notice that model 2 gave better values of film cooling effectiveness than that of the other models near the hole exit for all BR. In the downstream

region at (BR=0.5), model 3 gave higher value of ($\eta_{sa}$) than that of the other models, but for cases (BR=1 and 1.5), model 1 gave better performance for approximately (X/D $\geq$7).

The overall average film cooling effectiveness for the entire selected area $A_o$ ($\eta_{av}$) was calculated from the values of local film cooling effectiveness ($\eta$) for the entire pixels values included by the area ($A_o$). Figure 13 shows the effect of the blowing ratio on the averaged film cooling effectiveness ($\eta_{av}$) for the same cases. This Figure shows that model (1) gave higher value of ($\eta_{av}$) than other models, especially at high blowing ratio. It appears that the averaged film cooling effectiveness increases slightly with increasing BR, in models 1 and 2, while it decreases with increasing (BR) in model 3.

The average of the local heat transfer coefficient ratios (h / $h_o$), in which (h and $h_o$) represent the heat transfer coefficient on the plate surface with and without film cooling respectively are presented in Figure 14.This figure shows that model 1 gaves high (h/ho) with respect to the other two models at high blowing ratio.

In the practical application, turbine designers are concerned with the reduction of heat load to the film protected surface. The heat load can be presented by combining film cooling effectiveness ($\eta$) and the heat transfer coefficient ratio (h/$h_o$), according to equation (7), therefore the ratio (q/$q_o$) can be calculated. (q/$q_o$) represent the reduction in heat flux at the tested surface with the presence of coolant air. If the values of these ratios are less than 1, then the film coolant is beneficial according to Ref. **[5]**, while if the values are greater than 1, therefore effect of the film coolant is poor.Figure 15 represents the effect of blowing ratio on the overall heat flux ratios (q/$q_o$). It appears that the BR effect dominates the holes direction effects.

### Conclusions

The present work has reached to the following conclusions:

Numerical prediction of the flow field structure for holes arrangement shows that the vortices (counter pair kidney vortex and horseshoe vortex) both have major effects on cooling performance.

The reverse flow from backward injection hole creates pair of vortex similar to the kidney vortex created from forward injection hole, but in a plane parallel to the main stream.

Near the exit holes area, model 2 (opposite direction rows hole) shows uniform heat protection from the hot gas streams.

For low blowing ratio, the film cooling effectiveness is constructed at the holes exit region, while at high blowing ratio, the coolant jets developed downstream give better film

cooling effectiveness. On the other hand, model 3 arrangement (staggered rows, both inclination angles in the stream line direction) show an odd behavior.


**Nomenclatures**

$A_o$ selected area.

BR      blowing ratio

CFD Computational Fluid Dynamic

CVP Counter rotating vortex pair

$(CVP)_P$ Counter rotating vortex pair in parallel plan to main stream

D      film hole diameter

Exp. Experimental

h      heat transfer coefficient with coolant injection**.**

$h_o$ heat transfer coefficient without coolant injection**.**

K thermal conductivity of test surface.

q      heat flux with coolant injection.

$q_o$ heat flux without coolant injection.

T time when the IR image was captured.

$T_c$ coolant air temperature

$T_f$ film temperature

$T_i$      initial temperature

$T_m$ mainstream temperature

$T_w$ wall temperature

$U_c$      coolant air velocity

$U_m$      mainstream air velocity

η      film effectiveness

$η_{sa}$ spanwise average film cooling effectiveness

$η_o$      average film cooling effectiveness

Ø      overall cooling effectiveness

∝ thermal diffusivity

Ɣ      orientation angle

Θ      inclination angle

## References

[1]Han, J.C. andEkkad, S.V., " Recent Development in Turbine Blade Film Cooling", International Journal of Rotating Machinery, Malaysia, Vol. 7, No. 1, 2001, pp. 21-40.

[2] Ahn, J., Jung, I.S., and Lee, J.S., "Film cooling from two rows of holes with opposite behavior and adiabatic film cooling effectiveness", International Journal of Heat and Fluid Flow, Vol. 24, 2003, pp. 91-99.

[3]Dhungel, A., Phillips, A., Ekkad, S.V., and Heidmann, J.D., 2007, "Experimental Investigation of a Novel Anti-Vortex Film Cooling Hole Design", ASME IGTI Turbo Expo, Montreal, Paper GT 2007-27419.

[4] Lu, Y.,Dhungel, A.,Ekkad, S.V., and Bunker, R.S., 2007, "Effect of Trench Width and Depth on Film Cooling from Cylindrical Holes Embedded in Trenches", ASME Paper GT 2007-27388.

[5] Lu, Y., Dhungel, A., Ekkad, S.V., and Bunker, R.S., 2007, "Film Cooling Measurements for Cratered Cylindrical Inclined Holes", ASME Paper GT 2007-27386.

[6] Alwan, M.Sh., 2012," Experimental and Numerical Investigation of Film Cooling Thermal Performance for Staggered Rows of Circular Jet" PhD thesis, Mechanical Engineering Department , University of Technology.

[7] Holman, J.P. and Bhattacharyya, S., "Heat Transfer", Ninth Edition, New Delhi, McGraw-Hill, 2008.

[8] Ekkad, S.V., Ou, S., and Rivir, R.V., "A Transient Infrared Thermography Method for Simultaneous Film Cooling Effectiveness and Heat Transfer Coefficient Measurements from a single test", GT 2004-54236, Proceedings of ASME Turbo Expo 2004, Vienna, Austria.

[9] Ekkad, S.V., and Zapata, D., "Heat transfer coefficients Over a Flat Surface with Air and CO2 Injection Through Compound Angle Holes Using a Transient Liquid Crystal Image Method", ASME Journal of Turbomachinery Vol. 119, No. 3, 1997, pp. 580-586.

[10] Albert, J.E., Cunha, F. and Bogard, D.G., 2004, "Adiabatic and Overall Effectiveness for a Film Cooling Blade", ASME Paper GT2004-53998.

[11] Kline, S.J. and McClintock, F.A., 1953, " Describing uncertainties in single sample experimental", Mechanical Engineering, Vol. 75, pp. 3-8.

[12] Versteeg, H.K. and Malalasekera, W., 1996, "An introduction to  computational fluid dynamics the finite volume method", Longman Group, London.

[13] *Öztürk E.*, 2004, "CFD analysis of heat sinks for CPU cooling with FLUENT", MSc thesis, graduate school of natural and applied sciences, Middle East Technical University.

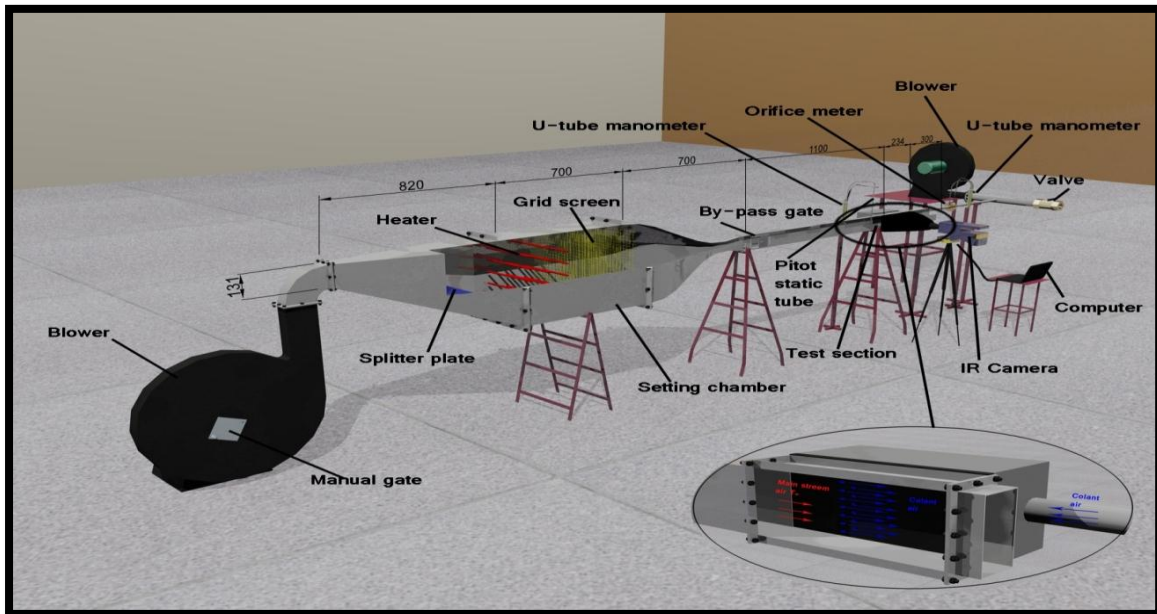[14] Jones, D.A. and Clarke, D.B., 2005, "Simulation of a wind-body junction experiment using the fluent code", DSTD-TR-1731, Australia.
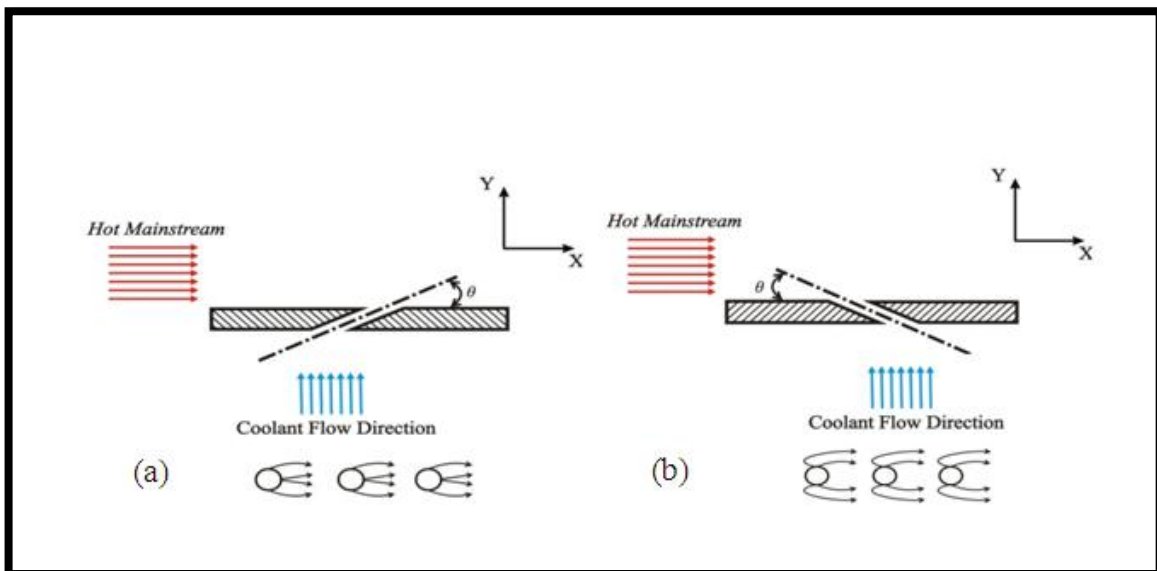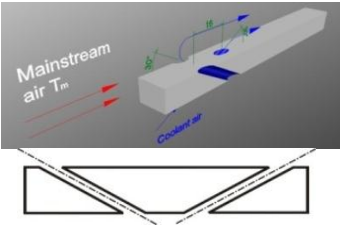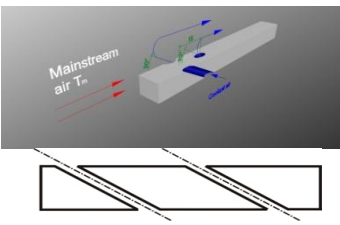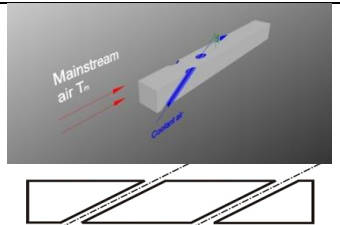


Figure 1 Schematic of the test rig



Figure (2) Illustrate diagram of the inclination and orientation angle:(a) $\theta = 30°$ and $\gamma = o°$, (b) $\theta = 30°$ and $\gamma = 180°$

Table (1) illustrated geometry for the three models.

| Model Number | Upstream Row | | Downstream Row | | Shape |
|---|---|---|---|---|---|
| | $\theta$ | $\gamma$ | $\theta$ | $\gamma$ | |
| **Model1** Stagger | 30° Acute jet angle | 180° | 30° Acute jet angle | 0° |  |
| **Model2** Stagger | 30° Acute jet angle | 180° | 150° Obtuse jet angle | 180° |  |
| **Model3** Stagger | 150° Obtuse jet angle | 0° | 30° Acute jet angle | 0° |  |
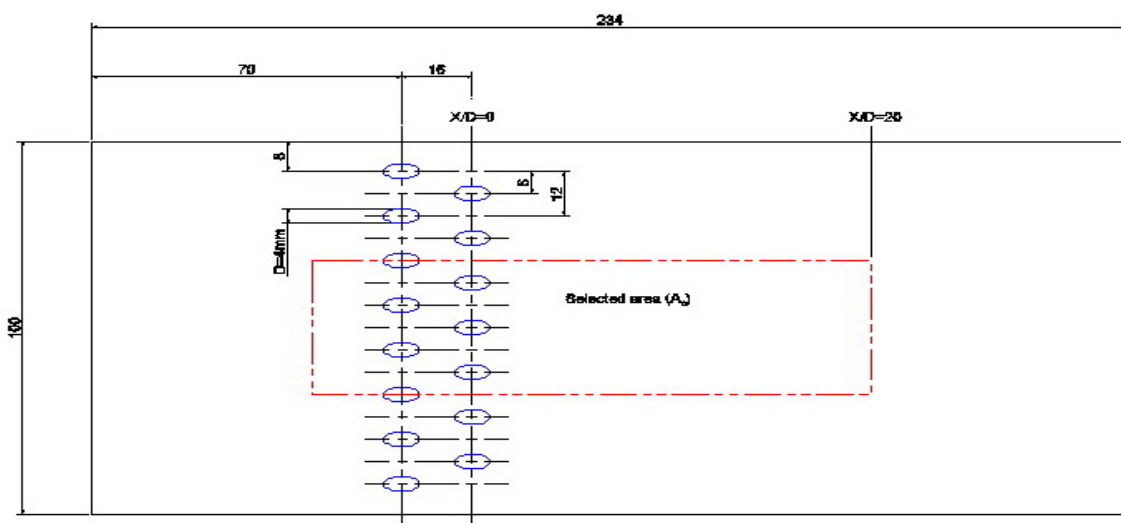


Figure 3 the middle selected area of the test section ($A_o$)
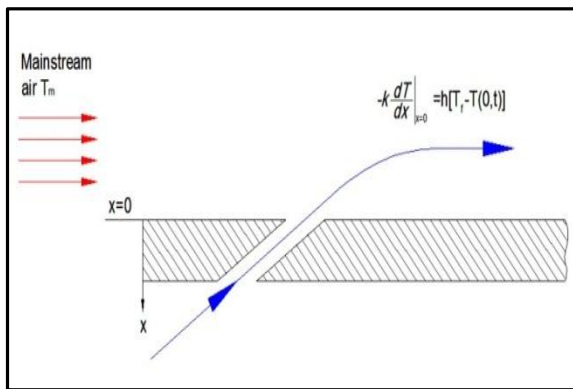
Figure 4 Flow over a flat plate
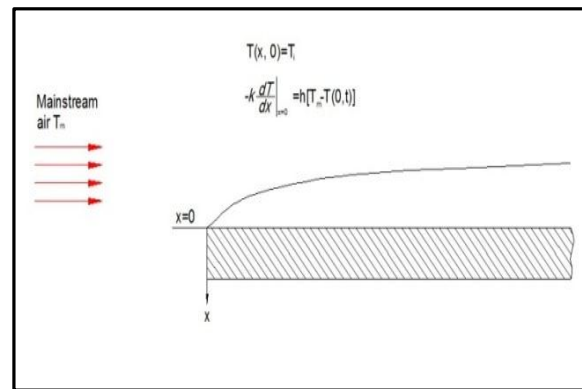


Figure 5 Film cooling over a flat plate
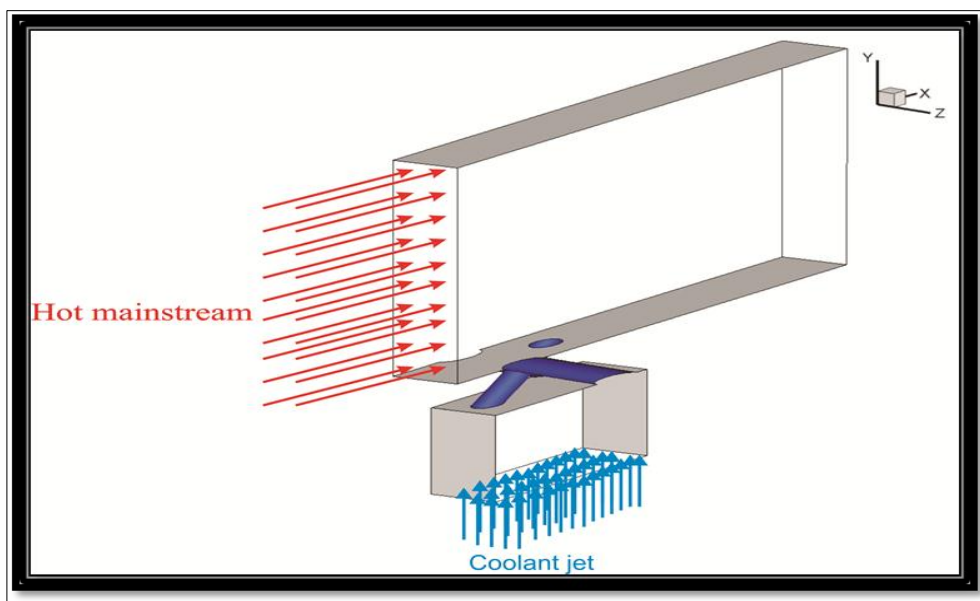


Figure 6 Schematic of geometry shape
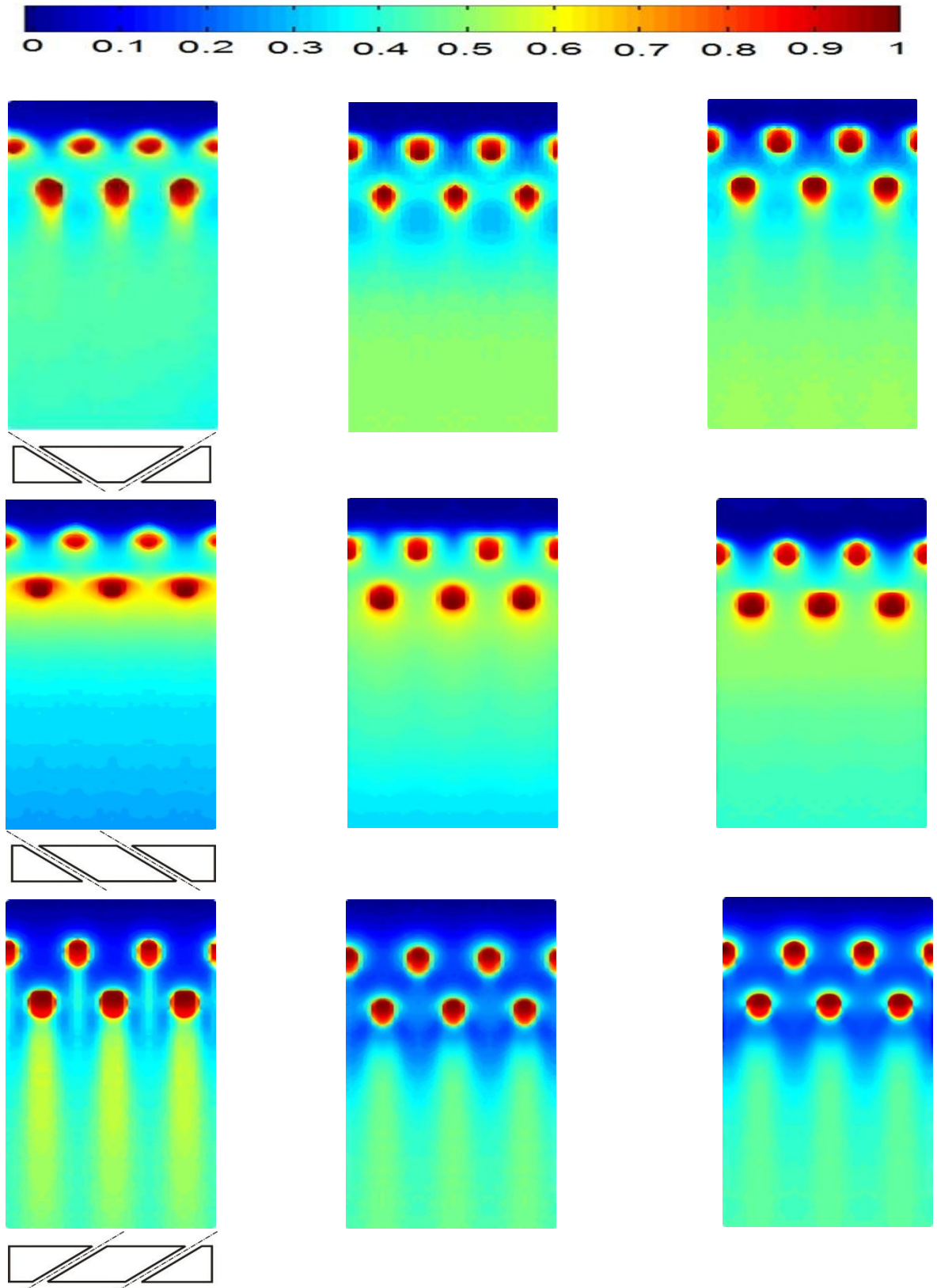
Figure 7 Contours of film cooling effectiveness for models (1, 2 and 3) at different blowing. (Exp.)
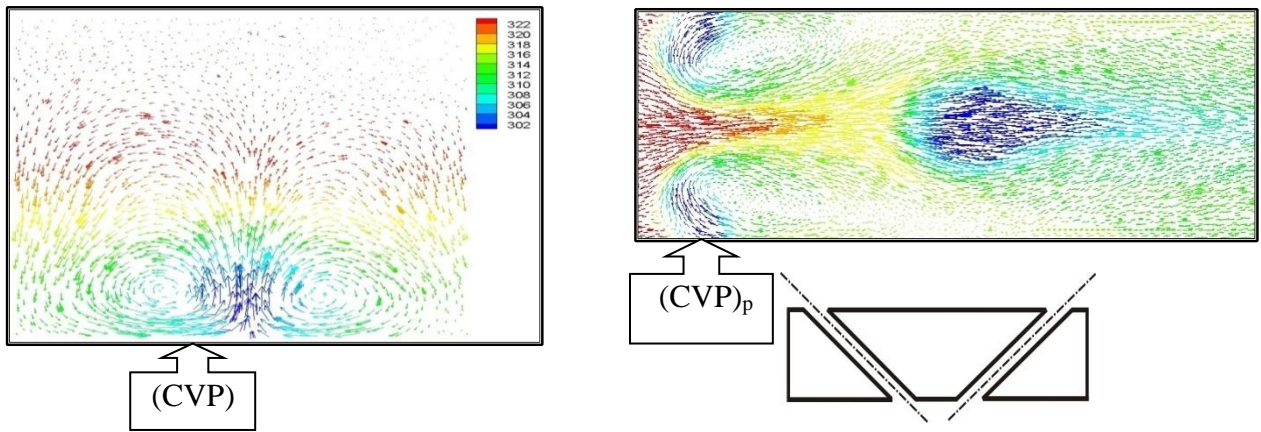
Figure 8 (a) Flow vectors colored by temperature at plane (X/D=4) for model 1at BR=1.5 (CFD)

(b) Flow vectors colored by temperature at plane parallel to test surface (Y=1mm) for
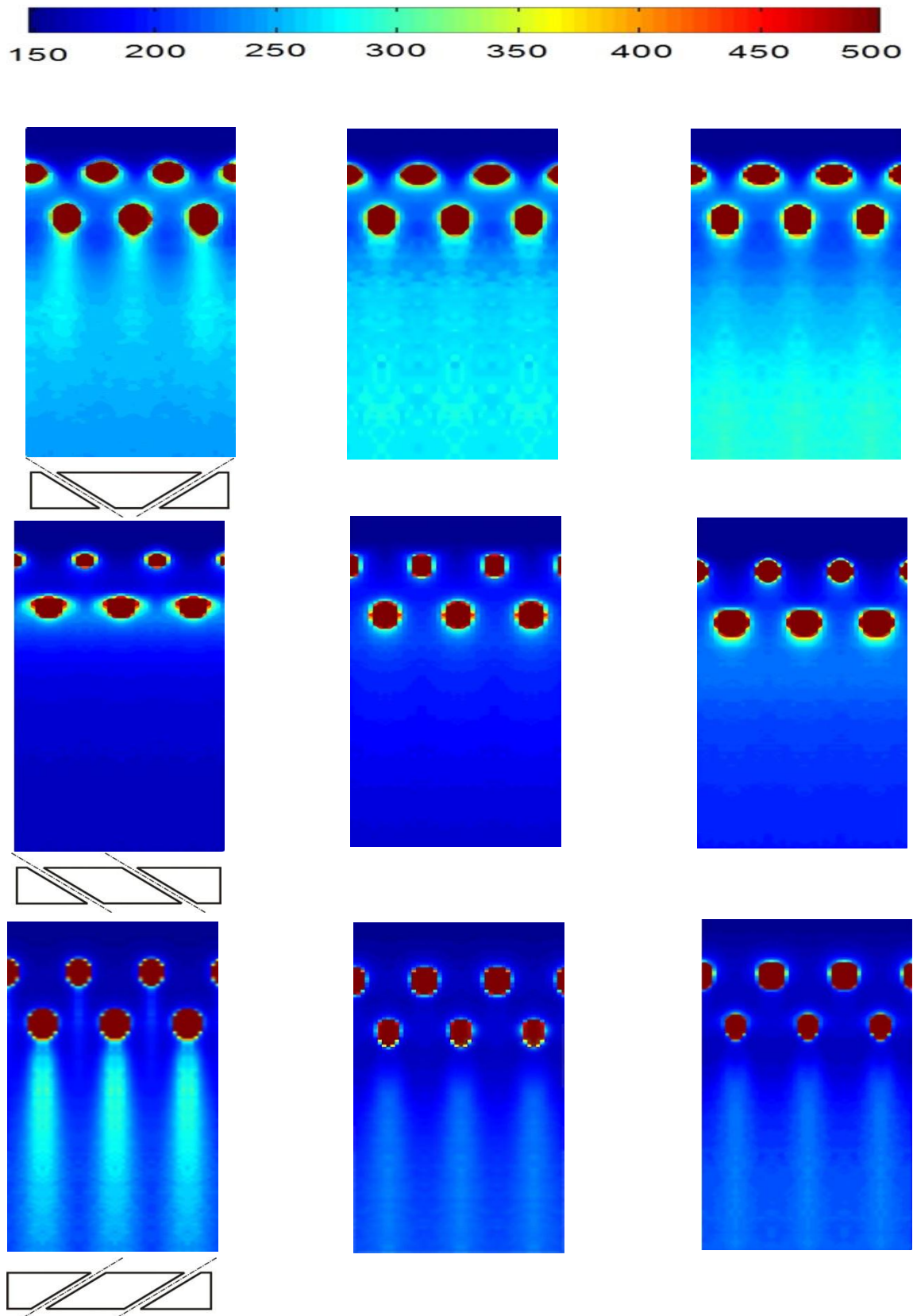
model 1 at BR=1.5. (CFD)
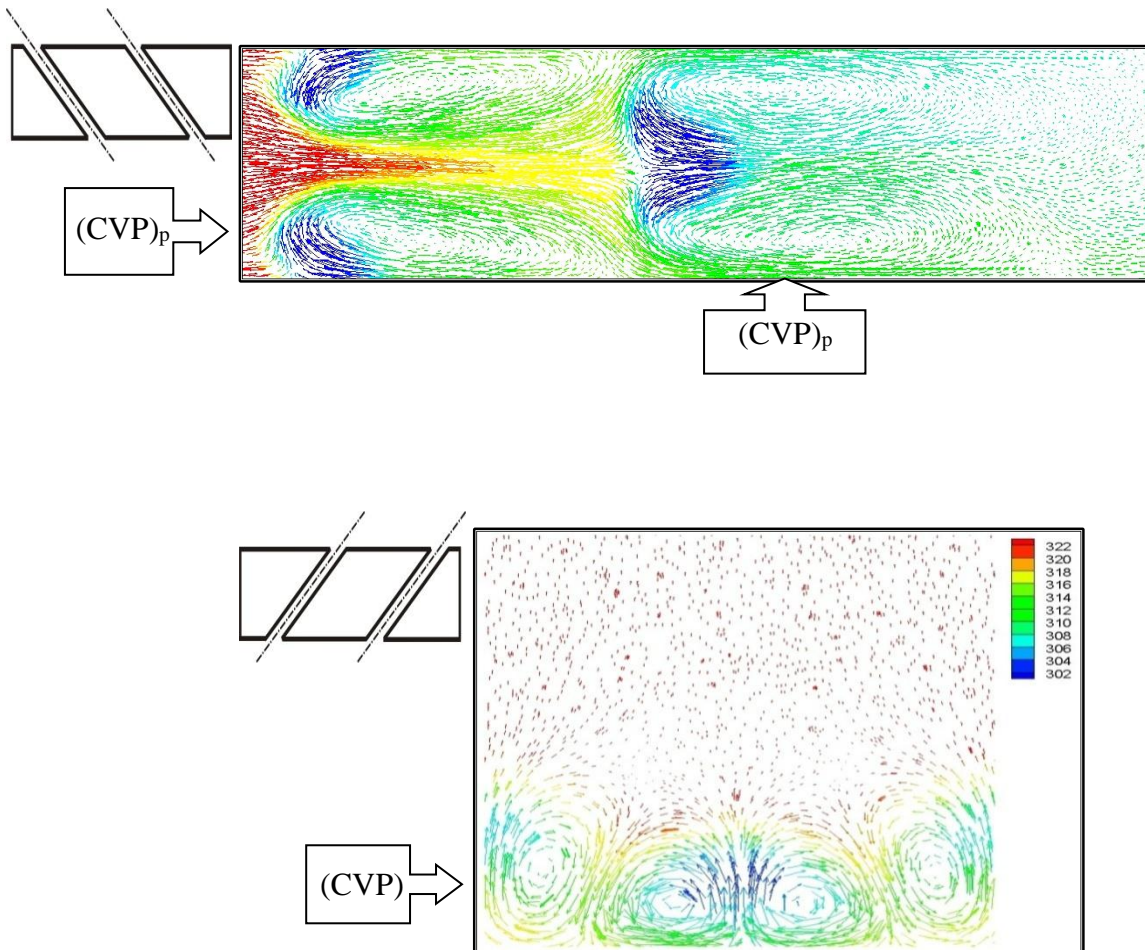
Figure 11 Contours of heat transfer coefficients (W/m$^2$.K) for models (1, 2 and 3) at different blowing ratio. (Exp.)
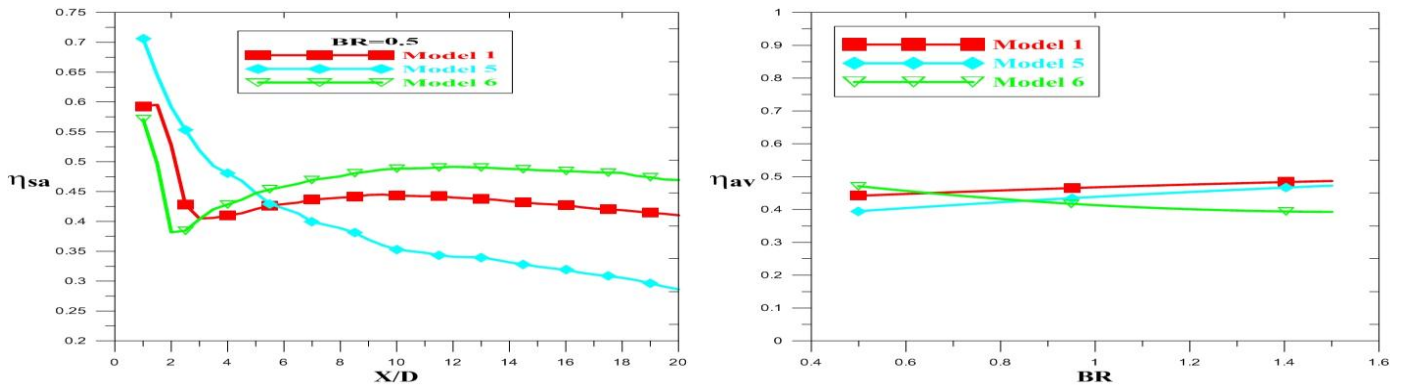
Figure 13 Effect of blowing ratios on averaged film cooling effectiveness for models (1, 2 and 3). (Exp.)
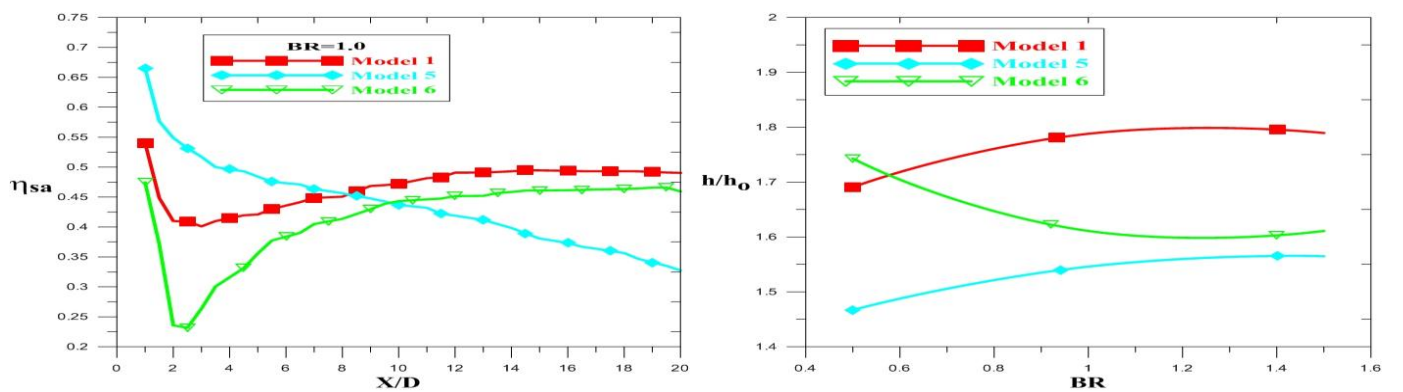


Figure 14 Effect of blowing ratios on averaged heat transfer coefficient ratios for models (1, 2 and 3). (Exp.)
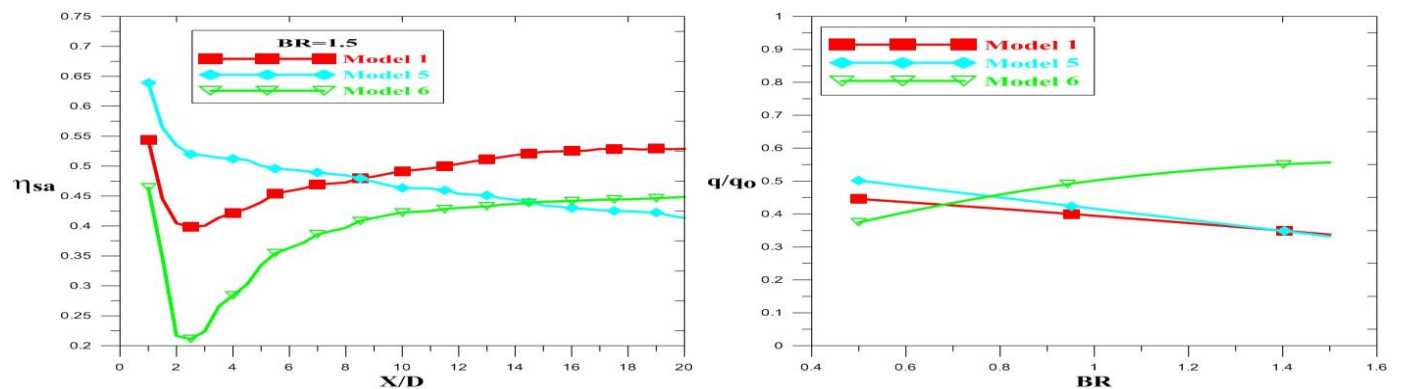


Figure 12 Effect of hole arrangement on span wise averaged film cooling effectiveness for models (1, 2 and 3) at:(a) BR=0.5, (b) BR=1.0, (c) BR=1.5. (Exp.)

Figure 15 Effect of blowing ratios on overall averaged heat flux ratios for models (1, 2 and 3). (Exp.)